Applied Catalysis B: Environmental 164 (2015) 297–304

Contents lists available at ScienceDirect

Applied Catalysis B: Environmental

journal homepage: www.elsevier.com/locate/apcatb

Single-crystalline $AgIn(MoO_4)_2$ nanosheets grafted Ag/AgBr composites with enhanced plasmonic photocatalytic activity for degradation of tetracycline under visible light

Xu Yan[a], Xiyou Wang[a], Wei Gu[a], MiaoMiao Wu[a], Yan Yan[a], Bo Hu[a], Guangbo Che[b], Donglai Han[c], Jinghai Yang[c], Weiqiang Fan[a,*], Weidong Shi[a,*]

[a] School of Chemistry and Chemical Engineering, Jiangsu University, Zhenjiang, 212013, PR China
[b] College of Environmental Science and Engineering, Jilin Normal University, Siping, 136000, PR China
[c] Key Laboratory of Functional Materials Physics and Chemistry of the ministry of Education, Jilin Normal University, Siping, 136000, PR China

ARTICLE INFO

Article history:
Received 12 July 2014
Received in revised form
18 September 2014
Accepted 21 September 2014
Available online 7 October 2014

Keywords:
Photocatalysis
Ternary metal molybdate
Plasmonic photocatalysts
Tetracycline degradation

ABSTRACT

Single-crystalline $AgIn(MoO_4)_2$ nanosheets have been successfully fabricated by facile hydrothermal method without any surfactants. Subsequently, Ag/AgBr-grafted $AgIn(MoO_4)_2$ nanosheets were synthesized by the in situ photoreduction of $AgBr/AgIn(MoO_4)_2$ composites prepared by a deposition–precipitation method. Under visible light irradiation. The $Ag/AgBr/AgIn(MoO_4)_2$ composites exhibit a strong absorbance in the visible region because of the surface plasmon resonance absorption of Ag nanocrystals. Compared with bare $AgIn(MoO_4)_2$ nanosheets, Ag/AgBr nanoparticles and $Ag/AgIn(MoO_4)_2$ composites, a dramatic enhancement in the degradation rate of tetracycline (TC) is observed over the $Ag/AgBr/AgIn(MoO_4)_2$ composites. The immense enhancement of the photocatalytic activity is attributed to the extended absorption in the visible-light region, effective charge separation, and synergistic enhancement induced by surface plasmon resonance (SPR) in the heterostructured $Ag/AgBr/AgIn(MoO_4)_2$. This study provides new insight into the fabrication of highly efficient and stable ternary metal molybdate based plasmonic photocatalysts and facilitates their practical application to solve environmental issues. The mechanism for the photodegradation of TC over $Ag/AgBr/AgIn(MoO_4)_2$ is discussed in detail.

1. Introduction

The growing energy and environmental issues have stimulated intensive researches in terms of solar energy conversion [1]. As a promising technique for environmental remediation, photocatalytic oxidation technique based on semiconductors has received much attention [2–5]. However, the photocatalytic activity of most photocatalysts available so far is still low, and some drawbacks still limit their practical applications, such as the limited utilization of visible light, fast recombination of photo-induced charge-carriers and the lack of reactive sites [6]. Therefore, the development of efficiently visible-light-driven (VLD) photocatalysis in terms of environmental remediation is still an great challenge. To date, the coupling of semiconductors with other semiconductors and/or metal on the nanoscale has been reported to greatly improve their photocatalytic performances, which have been considered as a potentially promising avenue to overcome these defects [7–10].

Very recently, the metal molybdates have attracted a tremendous amount of attention because of their promising technological importance in wide range of applications [11–15]. Due to their favorable electrochemistry, optical performances and unique structures, a large number of metal molybdates as photocatalysts have been explored [16–20]. Multi-metal oxides, one candidate to overcome the intrinsic limitations of single or binary metal oxides, show a significant improvement in either band gap reduction or band edge position [21]. However there are only a few reports on nano-scale double metal molybdates [22–25]. As a ternary metal molybdate, $AgIn(MoO_4)_2$ has the tetragonal structure with strong anisotropy and a band gap of 2.25 eV, which make it has great potential to be a novel visible-light-driven photocatalyst. However, no studies on the photocatalytic activities of single-crystalline $AgIn(MoO_4)_2$ nanostructures and their hetero-nanostructures have reported to date. To meet the requirements of future environmental and energy technologies, it is still necessary to design more

* Corresponding authors. Tel.: +86 511 8879 0187; fax: +86 511 8879 1108.
E-mail addresses: fwq4993329@163.com (W. Fan), swd1978@ujs.edu.cn (W. Shi).

http://dx.doi.org/10.1016/j.apcatb.2014.09.046
0926-3373/

novel VLD photocatalyst systems to further improve photocatalytic efficiencies.

Recently, a series of new hybrid photocatalysts on the basis of surface plasmon resonance (SPR) of metal nanoparticles (NPs) [26–28] were developed to decompose various organic pollutants under visible-light irradiation. It is considered to be a simple and ideal way to improve the photocatalytic performance of semiconductor photocatalysts by enhancing the light absorption and photo generated electrons transfer [29,30]. Meanwhile, since AgX can be in situ partially converted to plasmonic Ag nanoparticles, the interface between AgX and in situ-formed Ag is clean and well-defined, and the absorption coefficient of the resulting nanocomposites in the visible region can be significantly enhanced, which make Ag@AgX exhibit high photocatalytic activity and stability [31,32], and many efficiently plasmonic photocatalysts on the basis of silver halides have been frequently reported [33–37]. Therefore, Ag/AgBr modified $AgIn(MoO_4)_2$ composites are highly possible to be an ideal system with an improved optical absorption and separation efficiency of photogenerated charge carriers.

Herein, we report for the first time a successful attempt at the fabrication of the single-crystalline $AgIn(MoO_4)_2$ nanosheets through a facile template-free hydrothermal method. A facile method for growing Ag/AgBr nanoparticles on the $AgIn(MoO_4)_2$ nanosheets is developed by photoreducing $AgBr/AgIn(MoO_4)_2$ hybrids prepared by deposition-precipitation method. The as-prepared $Ag/AgBr/AgIn(MoO_4)_2$ composites exhibit remarkably enhanced plasmonic photocatalytic activity toward TC compared with Ag/AgBr, $Ag/AgIn(MoO_4)_2$ and pure $AgIn(MoO_4)_2$ crystals under visible light irradiation. This enhancement is ascribed to the surface plasmonic effect of Ag NPs and efficiently charge transfer. Furthermore, the tentative photocatalytic mechanism for the degradation of tetracycline over $Ag/AgBr/AgIn(MoO_4)_2$ composites is also discussed in detail.

2. Experimental

2.1. Materials and reagents

The reference reagents were obtained from Aladdin (China). All chemical were analytical grade without further purification and the deionized water was used throughout the study.

2.2. Synthesis of sample

The $AgIn(MoO_4)_2$ nanosheets was fabricated in a classical hydrothermal method. In a typical synthesis, 0.084 g, 0.5 mmol $AgNO_3$ and 0.191 g, 0.5 mmol $In(NO_3)_3$ were dissolved into 10 mL deionized water, after vigorous stirring for 15 min, 10 mL, 0.1 M Na_2MoO_4 solution dropwise add into the above solution and the pH of the mixture was adjusted into 3–8 using NaOH and HNO_3 solution. After vigorous stirring for another 20 min, the obtained mixture was transfer to a Teflon-lined stainless steel autoclave (50 mL in volume). Subsequently, hydrothermal treated in an air-flow electric oven at 180 °C for 24 h. After cooling down naturally, the orange-yellow precipitate was collected by centrifugation and thoroughly with deionized water and ethanol for several times, until a supernatant pH of 7 and then dried at 60 °C in air.

To deposit the Ag on $AgIn(MoO_4)_2$ nanosheets, certain amount $AgNO_3$ (mass ratios of $AgNO_3$ to $AgIn(MoO_4)_2$ was 0.5%, 2%, 4%, 6%, 8%, 10%) and $AgIn(MoO_4)_2$ add to 30 mL deionized water, and the suspension was sonicated for 30 min, after stirring for another 40 min to reach complete adsorption of Ag^+ on the surface of $AgIn(MoO_4)_2$ nanosheet. After that, the photodeposition step carried out under the irradiation of two 150 W tungsten halogen lamps for 1 h. Then the product thus obtained was centrifugation subsequently washed with deionized water and dried at 60 °C for 12 h. According to this method, different mass ratios of $Ag/AgIn(MoO_4)_2$ at 0.5%, 2%, 4%, 6%, 8% and 10% were prepared and denoted as 0.5-Ag, 2-Ag, 4-Ag, 6-Ag, 8-Ag and 10-Ag, respectively. For comparison, $Ag/AgBr/AgIn(MoO_4)_2$ sample was also constructed by adding the same molar ratio of KBr and $AgNO_3$ into $AgIn(MoO_4)_2$ suspension. The photodeposition step and samples collection step is similar to the preparation of $Ag/AgIn(MoO_4)_2$. Ag-AgBr photocatalyst is prepared by the detailed procedure reported by Geng et al. [38].

2.3. Characterization of the as-prepared samples

All of the powder X-ray diffraction (XRD) patterns were obtained on a D/MAX-2500 diffract meter (Rigaku, Japan) using Cu Ka radiation source ($k = 1.54056$) at a scan rate of 5° min^{-1} to determine the crystal phase of the obtained samples. The accelerating voltage and the applied current were 50 kV and 300 mA, respectively. Transmission electron microscopy (TEM), high resolution transmission electron microscopy (HRTEM) also has been used to characterization the samples. UV–vis diffused reflectance spectra of the samples were collected on a UV–vis spectrophotometer (UV2550, Shimadzu, Japan). $BaSO_4$ was used as a reflectance standard. The X-ray photoelectron spectroscopy (XPS) analyses of the samples were carried out on an S-520/INCA 300 spectrometer using 300 W Mg-Kα radiation, and the binding energies were referenced to the C1s line at 284.8 eV from adventitious carbon. Electrochemical impedance spectroscopy (EIS) was performed in a 0.1 M KCl solution containing 5 mM $Fe(CN)_6^{3-/4-}$ with a frequency range from 0.01 Hz to 10 kHz at 0.23 V, and the amplitude of the applied sine wave potential in each case was 5 mV which was taken with a ZENNIUM electrochemical workstation (Zahner Instruments, Germany). Electrochemical signals were recorded using a CHI660 B electrochemical analyzer (Chen Hua Instruments, Shanghai, China). All electrochemical and EIS curves were recorded using a conventional three-electrode system where a glassy carbon electrode (GCE, 3 mm in diameter) was used as a working electrode, a Ag/AgCl (saturated KCl solution) as a reference electrode and platinum wire as a counter electrode, respectively. The electrochemical measurements were performed in the potential range of 0–1.6 V with a scan rate of 100 mV s^{-1}.

2.4. Photocatalytic experiments

Photocatalytic activities of the photocatalysts were evaluted by degrading tetracycline (TC), using a photochemical reactor with visible light irradiation (500 W Xe lamp with a cut-off filter of 400 nm). In each experiment, 100 mg photocatalyst was added into TC aqueous solution (10 mg/L, 100 mL). Before illumination, the suspensions were magnetically stirred in the dark for 30 min to ensure the establishment of an adsorption–desorption equilibrium between the photocatalyst and TC. The sampling analysis was conducted in 10 min interval and a 3 mL suspension was sampled and centrifuged to remove the photocatalyst particles. The photocatalytic degradation ratio (DR) was calculated by the following formula:

$$DR = \left(1 - \frac{A_i}{A_0}\right) \times 100\%$$

A_0 is the initial absorbency of TC that reached absorption equilibrium, while A_i is the absorbency after the sampling analysis.

2.5. Electrochemical measurements

Prior to modification, the GCE was firstly polished with sand paper followed by 1.0, 0.3, and 0.05 mm alumina slurry, respectively, and then sonicated in water to remove any residues. The

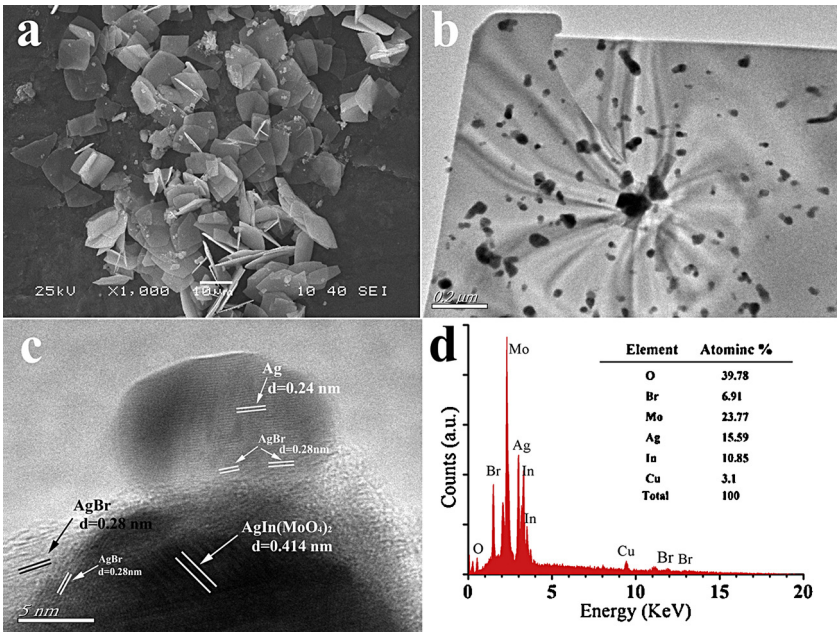

Fig. 1. FESEM image of $AgIn(MoO_4)_2$ nanosheets (a), and TEM (b), HRTEM (c), EDX (d) of $Ag/AgBr/AgIn(MoO_4)_2$.

procedure for the preparation of the modified electrodes was described as follows: 2.0 mg $AgIn(MoO_4)_2$ photocatalyst was dispersed in 1 mL ultrapure water to make a $AgIn(MoO_4)_2$ homogeneous suspension, then 6 μL of this suspension was cast onto the pretreated GCE surface and dried in air at room temperature to form the $AgIn(MoO_4)_2$ modified GCE. The $AgIn(MoO_4)_2$-GCE was rinsed with water several times prior to use. As a comparison, 6 μL of 2.0 mg mL^{-1} suspensions of $Ag/AgIn(MoO_4)_2$, $Ag/AgBr/AgIn(MoO_4)_2$, Ag/AgBr were used to fabricate the $Ag/AgIn(MoO_4)_2$-GCE, $Ag/AgBr/AgIn(MoO_4)_2$-GCE, Ag/AgBr-GCE, respectively.

3. Results and discussion

3.1. Morphology and structure of prepared photocatalysts

In the SEM image of $AgIn(MoO_4)_2$ nanosheet (Fig. 1a), it can be clearly observed that the potocatalysts has a square like morphology and high dispersion. The magnified TEM image (Fig. 1b) shows that the sample has a high crystallinity and deposited with Ag/AgBr nanoparticles on the surface of nanosheets. The HRTEM image (Fig. 1c) was recorded on the edge of Ag nanoparticles and $AgIn(MoO_4)_2$ nanosheet with the clear sight of AgBr. This result indicates that AgBr can be in situ partially converted to plasmonic Ag nanoparticles under UV irradiation, the interface between AgBr and in situ-formed Ag is clean and well-defined. The characteristic lattice fringe of 0.24 nm, 0.288 nm, 0.414 nm correspond to {1 0 1}, {2 0 0}, {1 0 5} size of Ag, AgBr, $AgIn(MoO_4)_2$, respectively. To further confirm the existence of Ag, the area with the nano-sheet were selected for EDX microanalysis. Fig. 1d depicted the EDX image of the as-prepared $Ag/AgBr/AgIn(MoO_4)_2$ photocatalyst, from which Ag, Br, In, O, Mo can be directly observed. The impurity signals of C and Cu are attributed to the carbon-coated supporting copper grid, which is necessary in the HRTEM-EDX.

3.2. Influence of precursors pH on morphology and crystalline

To demonstrate the effect of the pH value on the formation of $AgIn(MoO_4)_2$ nanostructure, pH dependent SEM and XRD analyses were conducted by adjusting the pH value of the precursor without changing other influencing factors, and the results are shown in Figs. 2 and 3, respectively. As shown in the pH-dependent SEM patterns, bulk, sheet assembled, and monodisperse samples obtained with the precursor pH at 3, 4, 5, respectively. When the pH value is increased up to 6, the nanosheets break after hydrothermal with a same synthesis condition. Further increase the pH to 7 and 8, irregularity morphology products obtained. These prepared samples were also examined by XRD (Fig. 3) to further confirm the crystalline. The XRD result shows that, pH value has a significant influence on the formation of crystallized $AgIn(MoO_4)_2$ and on the particular pH range formation. The result shows that, $AgIn(MoO_4)_2$ crystallized easily with a acidic condition, further increase the precursor pH to alkalinity, Ag_2MoO_4 (JCPDS card no. 75-0250) finally obtained.

3.3. Band structure

To explain the mechanism of action of the synthesised photocatalysts, the conduction band (CB) and valence band (VB) potentials of $AgIn(MoO_4)_2$ must be confirmed. From Fig. 4, it can also be seen that the absorption edge of $AgIn(MoO_4)_2$ sample is at about 550 nm in the spectrum. It is known that the optical absorption near the band edge for a crystal obeys the following equation [39]:

$$\alpha h\gamma = A(h\gamma - E_g)^n$$

where α, h, γ, A and E_g are the absorption coefficient, Planck constant, light frequency, proportionality and band gap, respectively, and n the properties of the transition in a semiconductor. On the basis of this equation, the band gap of $AgIn(MoO_4)_2$ counted is 2.25 eV.

For a semiconductor, CB and VB can be calculated according to the following empirical equation:

$$E_{VB} = X - E_e + 0.5E_g$$

$$E_{CB} = E_{VB} - E_g$$

where E_{VB} is the VB edge potential, X is the electronegativity of the semiconductor, which is the geometric mean of the electronegativity of the constituent atoms, E_e is the energy of free electrons

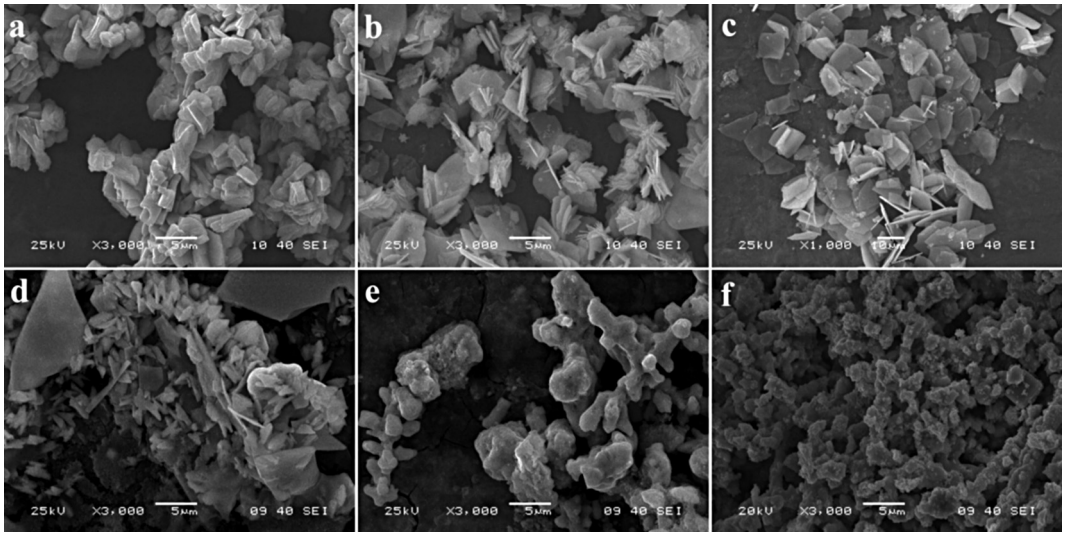

Fig. 2. Influence of precursors pH on morphology and crystalline: (a) pH 3; (b) pH 4; (c) pH 5; (d) pH 6; (e) pH 7; (f) pH 8.

on the hydrogen scale (about 4.5 eV), E_g is the band gap energy of the semiconductor, and E_{CB} is the CB band. The edge of the valence band (VB) of $AgIn(MoO_4)_2$ was determined to be +2.627 eV (vs normal hydrogen electrode, NHE), and the edge of the conduction band was estimated to be +0.377 eV (vs NHE).

3.4. Xrd of $AgIn(MoO_4)_2$ and plsmonic photocatalyst

The phase structure and crystallinity of the as-synthesized $AgIn(MoO_4)_2$ sample, and the plasmonic photocatalyst of AgBr/Ag- and Ag- deposited samples were characterized by XRD. As shown in Fig. 5, all of the samples exhibit some diffraction peaks that are assigned to the monoclinic $AgIn(MoO_4)_2$ (JCPDS card no. 36-0312), and no impurities are discernible. For all the three photocatalysts, the peaks at $2\theta^o$ about 26.7°, 31.1°, 44.6°, 55.4° can be indexed to the (1 1 1), (2 0 0), (2 2 0), and (2 2 2) of AgBr (JCPDS card No. 06-0438), respectively [40]. The peaks at $2\theta = 38.1$ for $Ag/AgIn(MoO_4)_2$ and $Ag/AgBr/AgIn(MoO_4)_2$ can be assigned to (1 1 1) plane of Ag^0 crystal (JCPDS card No. 65-2871). The absence of Ag^0 peaks in XRD patterns of $AgIn(MoO_4)_2$ indicates that the Ag^0 nanoparticles were formed after the UV irradiation. In addition, the peaks of silver and AgBr are not very high, this is determined by the content of silver and AgBr.

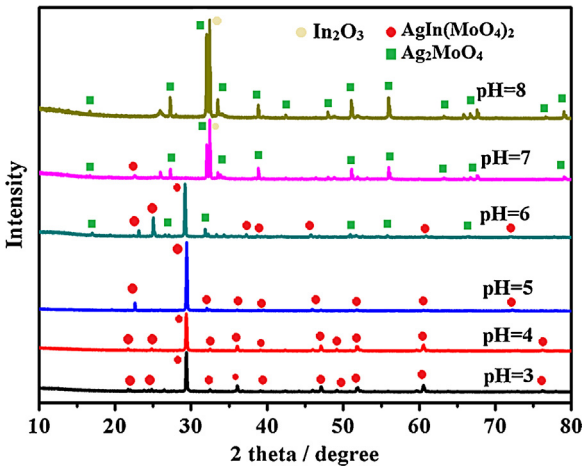

Fig. 3. XRD patterns of the as-prepared $AgIn(MoO_4)_2$ with the precursor pH from 3 to 8.

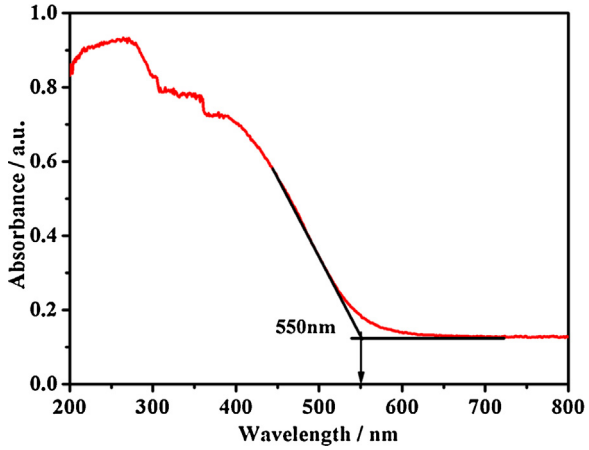

Fig. 4. The UV–vis adsorption curve of $AgIn(MoO_4)_2$ nanosheets.

3.5. UV–vis adsorption of prepared Ag- and Ag/AgBr-modified $AgIn(MoO_4)_2$

Considering the band structure plays a key role in determine the photocatalytic activity of semiconductors, the UV–vis diffused

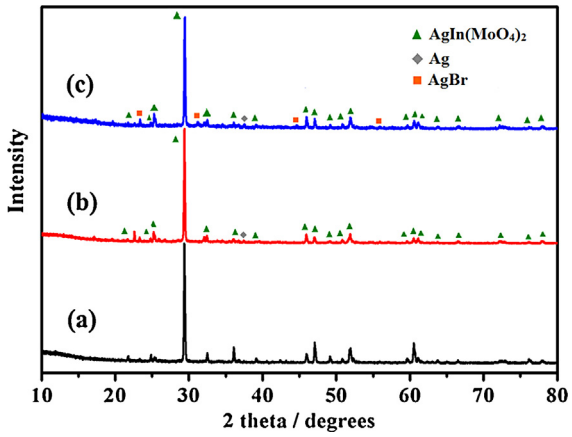

Fig. 5. XRD patterns of the as-prepared $AgIn(MoO_4)_2$ sample (a), $Ag/AgIn(MoO_4)_2$ (b), and $Ag/AgBr/AgIn(MoO_4)_2$ (c) plasmonic photocatalysts (6 wt% of deposited Ag content).

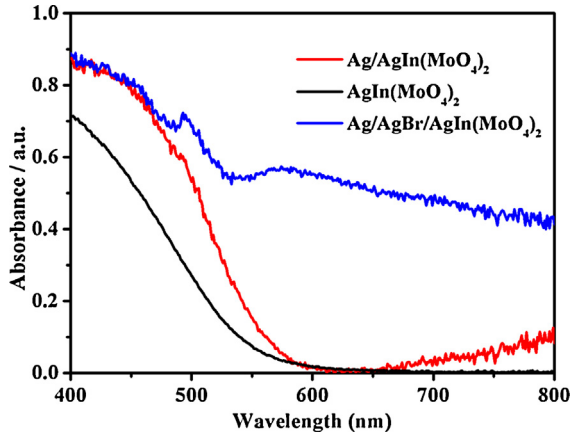

Fig. 6. UV–vis spectra of prepared $AgIn(MoO_4)_2$ and the optimal silver content plasmonic photocatalysts.

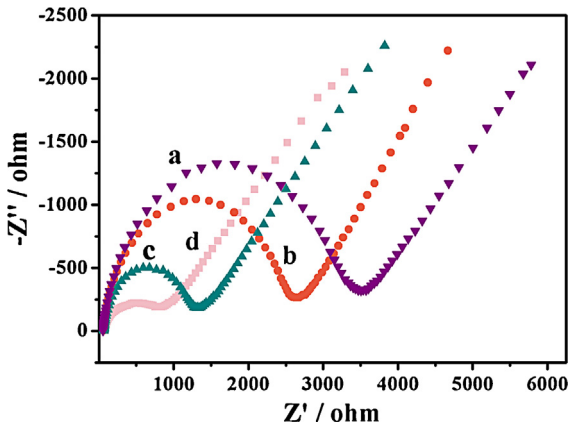

Fig. 8. EIS of $AgIn(MoO_4)_2$-GCE (a), $Ag/AgIn(MoO_4)_2$-GCE (b), Ag/AgBr-GCE (c) and $Ag/AgBr/AgIn(MoO_4)_2$-GCE (d) in 0.1 M KCl containing 5 mM $Fe(CN)_6^{3-/4-}$.

reflection spectra studies were performed. Fig. 6 shows the optical absorption of the prepared $AgIn(MoO_4)_2$, $Ag/AgIn(MoO_4)_2$, and $Ag/AgBr/AgIn(MoO_4)_2$ hybrids. Comparison with single $AgIn(MoO_4)_2$, both of the Ag or Ag/AgBr grafted $AgIn(MoO_4)_2$ photocatalysts exhibited a red-shift and a obviously enhanced light absorption in visible-light region. The strong and broad absorption larger than 450 nm should result from the strong SPR of Ag NPs. The $Ag/AgBr/AgIn(MoO_4)_2$ shows a strong SPR absorption in the range of 500–750 nm, which is caused by the SPR effect of Ag^0 particles and the light adsorption of AgBr. It is known that the SPR frequency depends closely on the size and shape of particles, interparticle spacing, and local dielectric environment [41]. Therefore, the observed change in $Ag/AgIn(MoO_4)_2$ could be ascribed to the increased proportion and size of Ag NPs.

3.6. XPS of $Ag/AgBr/AgIn(MoO_4)_2$ photocatalysts

The corresponding XPS spectra (Fig. 7) provide further structural information for the $Ag/AgBr/AgIn(MoO_4)_2$ nanosheets. In Fig. 7b, the Ag 3d spectra consisting of two individual peaks at 367.7 and 373.7 eV can be attributed to Ag 3d5/2 and 3d3/2 binding energies of metallic Ag and Ag (1). Because the Ag 3d photoelectron peaks are relatively insensitive to the oxidation state changes, it is barely distinguishable between Ag (0) and Ag (I) [40]. As shown in Fig. 7c, the peaks at 68.6 eV and 69.1 eV correspond to the Br 3d5/2 and Br 3d3/2, respectively, which agree with those of Br in AgBr [42]. Fig. 7d gives the XPS spectrum of O 1s region locating at 530.8 eV. Both the XRD and XPS results indicate that the above mentioned method is feasible to produce $Ag/AgBr/AgIn(MoO_4)_2$ composites.

3.7. Electrochemical impedance spectroscopy

Electrochemical impedance spectroscopy (EIS) measurements were also employed to investigate the charge transfer resistance and the separation efficiency between the photogenerated electrons and holes. Using $Fe(CN)_6^{3-/4-}$ as the electrochemical probe, the Nyquist plots of different electrodes were obtained (Fig. 8). Obviously, the charge transfer resistance

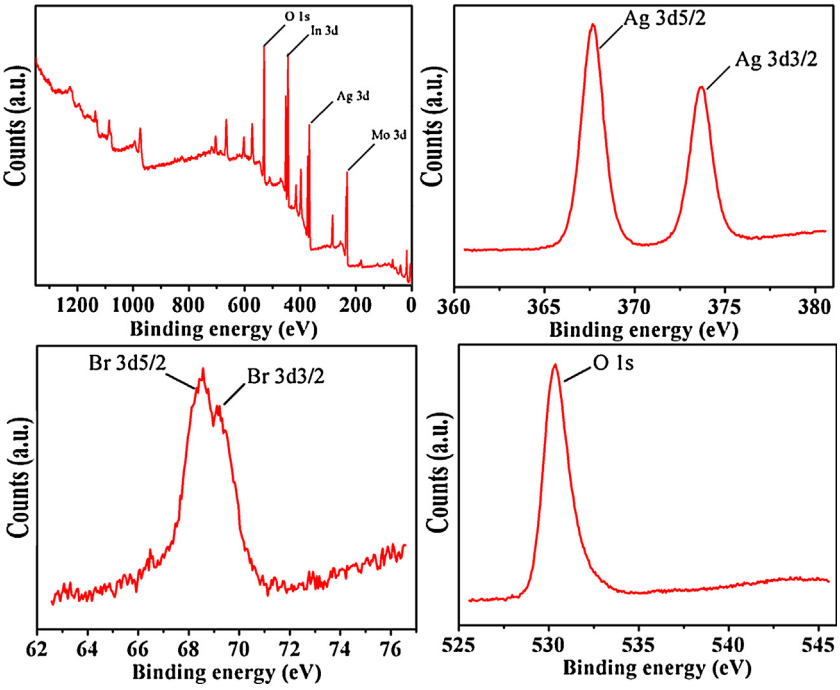

Fig. 7. XPS spectra of $Ag/AgBr/AgIn(MoO_4)_2$ photocatalysts.

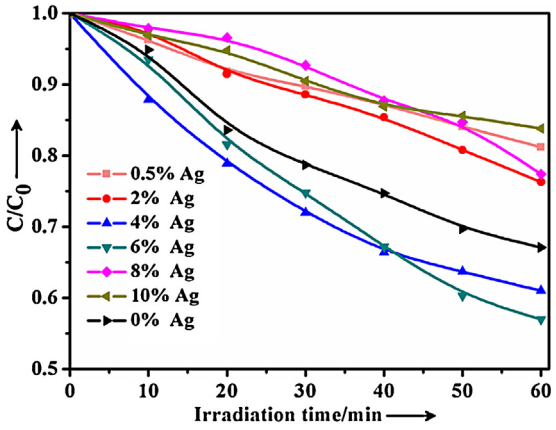

Fig. 9. Photocatalytic degradation curve of $AgIn(MoO_4)_2$ only modified by silver in different concentration.

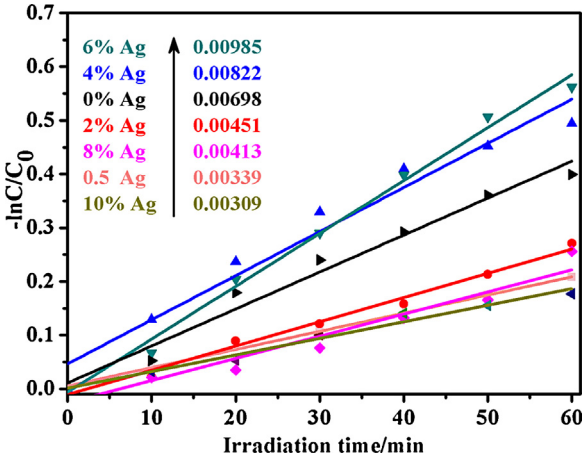

Fig. 10. The pseudo-first-order reaction kinetics of TC under visible light irradiation.

(Rct) at the Ag/$AgIn(MoO_4)_2$-GCE (curve b), Ag/AgBr/$AgIn(MoO_4)_2$-GCE (curve d) and Ag/AgBr-GCE (curve c) is smaller than that at the $AgIn(MoO_4)_2$-GCE (curve a). In addition, when Ag/AgBr/$AgIn(MoO_4)_2$ was incorporated into the electrochemical system, it was obvious that the R_{ct} is much smaller than other samples. Generally, the smaller the arc radius on the EIS Nynquist plot, the lower the charge transfer resistance. Thus, the EIS results demonstrated impedance order of prepare samples as Ag/AgBr/$AgIn(MoO_4)_2$-GCE < Ag/AgBr-GCE < Ag/$AgIn(MoO_4)_2$-GCE < $AgIn(MoO_4)_2$-GCE. The lowest impedance value for Ag/AgBr/$AgIn(MoO_4)_2$-GCE could indicate the excellent electron-transfer, which can inhibit the electron–hole recombination and beneficial to the enhanced photocatalytic activity.

3.8. Evaluation of photocatalytic activity

As a widely used antibiotic, tetracycline (TC) is usually released into the water environment [43] and directly affects the environment by disrupting the ecosystem equilibrium [44]. Photocatalytic degradation of TC provide a good tool for the degradation of antibiotics for the advantages of low cost, no secondary pollution, and environment friendly. To elucidate the photocatalytic activities of prepared photocatalysts, the photodegradation of TC experiment was carried out.

The photocatalytic activity of Ag/$AgIn(MoO_4)_2$ samples was evaluated by degradation of TC under visible-light irradiation, as shown in Fig. 9. After photocatalytic reaction for 1 h, all of the photocatalyst performed a degradation activity in TC degradation, and silver with an optimum constant of 6% reached the highest degradation ratio about 42%. Compare with bare single crystal $AgIn(MoO_4)_2$ nanosheets, an obviously enhancement revealed. This improvement attributes to the surface plasmon resonance of surface Ag NPs.

Fig. 10 shows that the photocatalytic degradation of TC by Ag/$AgIn(MoO_4)_2$ fits the pseudo-first-order kinetics, $\ln(C/C_0) = kt$, where C is the concentration of the TC at time t, C_0 is the initial concentration of the TC solution, and the slope k is the apparent reaction rate constant. It is obviously that the kinetic fitting curves with irradiation time (t) as the horizontal ordinate and $-\ln(C/C_0)$ as the vertical ordinate are close to linear correlations, which evinces that the photocatalytic degradation process of TC complies with the first-order reaction kinetic process. All the samples exhibit efficient photocatalytic activities under visible light irradiation. Among them, Sample 6% Ag/$AgIn(MoO_4)_2$ assumes highest photocatalytic activity in accord with photocatalytic result. It may be attributed to the optimum Ag amounts on the $AgIn(MoO_4)_2$ nanosheet, which is considered to the obviously enhancement of light adsorption and electron transfer.

Additionally, a comparison on the photocatalytic activity between Ag/AgBr, Ag/$AgIn(MoO_4)_2$, $AgIn(MoO_4)_2$ and a composite of Ag/AgBr/$AgIn(MoO_4)_2$ was conducted. As is shown in Fig. 11, it can be obviously seen that, the pure $AgIn(MoO_4)_2$ and AgBr shows a lower photocatalytic activity about 30% and 7%, respectively. After silver deposited, the activity increased, after 1 h reaction time under visible light, the degradation ratio reached 43%, this is attributed to the SPR effect of Ag NPs. The blank experiment result showed a can be ignored photolysis of TC. Moreover, the Ag/AgBr/$AgIn(MoO_4)_2$ composites with a optimal mass of 6% Ag showed a dramatically improved photocatalytic activity compared with AgBr, Ag/$AgIn(MoO_4)_2$ or $AgIn(MoO_4)_2$ alone, and the C/C_0 decreased from 1 to 0.35. Ag/AgBr/$AgIn(MoO_4)_2$ composites displayed perfect photocatalytic activity under direct sunlight irradiation, because silver bromide with a 2.6 eV band gap is very sensitive to sunlight, and the Ag^0 species on the surface of the catalyst probably enhances the electron–hole separation and the interfacial charge transfer.

3.9. Tentative photocatalytic mechanism

To further evaluate the role of reactive species, a series of quenchers were used to scavenge the relevant reactive species. Isopropanol (IPA) was added to the reaction system as an •OH scavenger [45], EDTA-2Na [46] was adopted to quench of h^+,

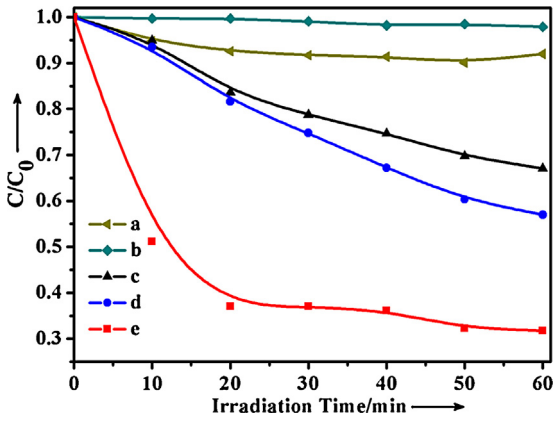

Fig. 11. The photocatalytic degradation of TC under visible light irradiation: (a) Ag/AgBr, (b) blank, (c) bare $AgIn(MoO_4)_2$ nanosheets, (d) Ag/$AgIn(MoO_4)_2$, (e) Ag/AgBr/$AgIn(MoO_4)_2$.

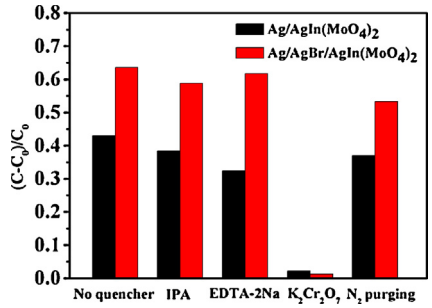

Fig. 12. Trapping experiment of active species during the photocatalytic reaction.

and $K_2Cr_2O_7$ was introduced as the scavenger for the photo-excited electrons [47]. Fig. 12 displays the trapping experiment of $Ag/AgIn(MoO_4)_2$ and $Ag/AgBr/AgIn(MoO_4)_2$ photocatalytic system. It can be seen that the photocatalytic degradation of TC was not affected by the addition of 1 mM isopropanol and EDTA-2Na. On the contrary, the photocatalytic degradation of TC is obviously inhibited after the addition of $K_2Cr_2O_7$. In addition, the degradation rate of $Ag/AgBr/AgIn(MoO_4)_2$ and $Ag/AgIn(MoO_4)_2$ under the anoxic suspension (N_2-saturated condition) is decreased to 53.3% and 39%, respectively. This result indicate that O_2 primarily acted as efficient electron traps, leading to the generation of $^{\bullet}O_2^-$. On the basis of these results, it can be concluded that electron play a significant role in the degradation of TC. Therefore, the photocatalytic mechanism of $Ag/AgBr/AgIn(MoO_4)_2$ hybrid might be a classic theory of Z-scheme, as discussed below.

Base on the above results, a possible Z-scheme pathway for the degradation of TC over $Ag/AgBr/AgIn(MoO_4)_2$ was proposed, as presented in Fig. 13. Under visible light ($\lambda > 420$ nm), $AgIn(MoO_4)_2$ and AgBr can be simultaneously excited to form electron–hole pairs, and the Ag NPs act as the charge transmission bridge to form the visible-light-driven $Ag/AgBr/AgIn(MoO_4)_2$ Z-scheme system. Compared with the single-electron reduction of oxygen ($O_2 + e^- + H^+ \leftrightharpoons HO_2(aq)$, −0.046 eV vs SHE) [48], it is clear that the CB electrons on $AgIn(MoO_4)_2$ cannot reduce oxygen effectively. Thus, after exited by visible light, the CB electrons of $AgIn(MoO_4)_2$ shift to Ag NPs due to its lower reduction power (+0.4 V vs SHE), and which is lower than the potential of Ag^+/Ag (+0.799 V vs SHE) [49]. Simultaneously, its VB holes remain on the VB to decompose TC. On the other hand, since the energy level of Ag is above the VB of AgBr, VB-holes (AgBr) also easily flow into metal Ag, which is faster than the electron–hole recombination between the VB and CB of AgBr [50]. Therefore, basic principle of electrons transfer and photocatalytic process on the $Ag/AgBr/AgIn(MoO_4)_2$ Z-scheme system might be as follows: CB-electrons of $AgIn(MoO_4)_2$ easily flow into metal Ag and recombine with the VB holes of AgBr. The high reducing electron located on the CB bottom of AgBr will react with molecular oxygen to form O^{2-} that can further oxidize TC.

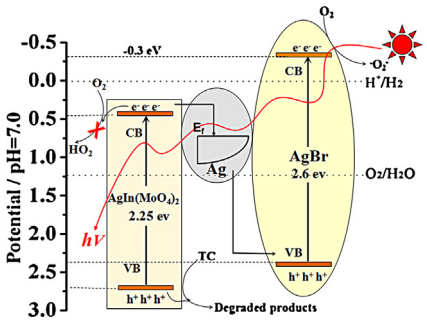

Fig. 13. Possible schematic diagram of the mechanism of the photocatalytic reaction on the $Ag/AgBr/AgIn(MoO_4)_2$ photocatalyst system.

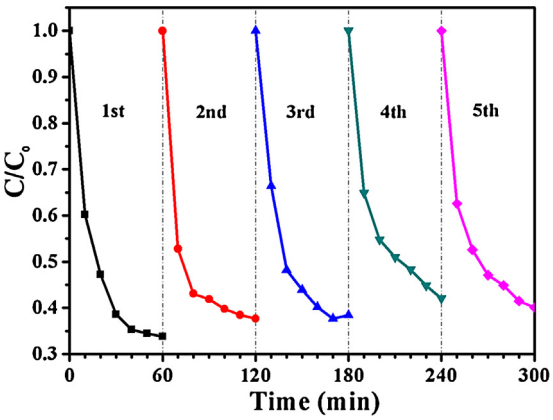

Fig. 14. Cycling runs in the photodegradation of TC (10 mg/L, 100 mL) at natural pH in aqueous dispersion containing 100 mg of $Ag/AgBr/AgIn(MoO_4)_2$ under visible-light illumination (6 wt% of deposited Ag content).

Moreover, the photogenerated holes could be scavenged by Br^- to produce Br_0 [51]. In addition, Br^0 is also an active species which can promote the reaction, and the Br^0 reduced to Br^- after the photocatalytic reaction.

Furthermore, the stability of the $Ag/AgBr/AgIn(MoO_4)_2$ photocatalyst was investigated through the cyclic degradation of TC under visible light irradiation, as presented in Fig. 14. The recycle test was performed five times on $Ag/AgBr/AgIn(MoO_4)_2$ 6% silver sample. 0.1 g catalyst was used in the recycling experiment. It can be clearly seen that the photocatalytic activity remained almost constant which proves the prepared $Ag/AgBr/AgIn(MoO_4)_2$ has high stability in the photocatalytic process under visible light irradiation. The incorporation of $Ag/AgBr$ into the $AgIn(MoO_4)_2$ nanosheets was therefore thought to enhance the visible light activity of $AgIn(MoO_4)_2$ and also inhibits the photo-corrosion of AgBr, leading to a stable and durable photocatalytic activity. Thus, $Ag/AgBr/AgIn(MoO_4)_2$ plasmonic photocatalyst is stable and recyclable during the photocatalytic process.

4. Conclusion

In this paper, $AgIn(MoO_4)_2$ nanosheet was synthesized by the facile hydrothermal method. $Ag/AgBr/AgIn(MoO_4)_2$ and $Ag/AgIn(MoO_4)_2$ plasmonic system were also constructed by a deposition-precipitation method. Their efficient photocatalytic activity, especially the three-component visible-light driven (VLD) photocatalysts could be widely used for environmental purification of organic pollutants in aqueous solution. In addition, the role of metallic Ag in $Ag/AgIn(MoO_4)_2$ and $Ag/AgBr/AgIn(MoO_4)_2$ were analyzed, and we found that the role of metallic Ag was SPR and the heterostructures bridge for $Ag/AgIn(MoO_4)_2$ and $Ag/AgBr/AgIn(MoO_4)_2$, respectively. It indicates that metallic Ag and $Ag/AgBr$ can effectively enhance the VLD photocatalytic activity.

Acknowledgements

We gratefully acknowledge the financial support of the National Natural Science Foundation of China (21276116, 21477050, 21301076, 21303074 and 21201085), Excellent Youth Foundation of Jiangsu Scientific Committee (BK20140011), Open Project of State Key Laboratory of Rare Earth Resource Utilizations (RERU2014010), Program for New Century Excellent Talents in University (NCET-13-0835), Henry Fok Education Foundation (141068) and Six Talents Peak Project in Jiangsu Province (XCL-025).

References

[1] C.C. Chen, W.H. Ma, J.C. Zhao, Chem. Soc. Rev. 39 (2010) 4206–4219.
[2] H. Tong, S. Ouyang, Y. Bi, N. Umezawa, M. Oshikiri, J. Ye, Adv. Mater. 2 (2011) 229–251.
[3] A.N. Banerjee, Nanotechnol. Sci. Appl. 4 (2011) 35–65.
[4] K. Nakata, A. Fujishima, J. Photochem. Photobiol. C: Photochem. Rev. 13 (2012) 169–189.
[5] Y. Xu, W. Zhang, ChemCatChem 5 (2013) 2343–2351.
[6] M. Kazuhiko, T. Kentaro, D. Kazunari, J. Catal. 254 (2008) 198–204.
[7] W. Zhou, H. Liu, J. Wang, D. Liu, G. Du, J. Cui, Appl. Mater. Interfaces 2 (2010) 2385–2392.
[8] G. Luo, X. Jiang, M. Li, Q. Shen, L. Zhang, H. Yu, Appl. Mater. Interfaces 5 (2013) 2161–2168.
[9] Y. Qu, X. Duan, Chem. Soc. Rev. 42 (2013) 2568–2580.
[10] C.L. Yu, G. Li, S. Kumar, K. Yang, R.C. Jin, Adv. Mater. 26 (2014) 892–898.
[11] A. Phuruangrat, N. Ekthammathat, T. Thongtem, S. Thongtem, J. Phys. Chem. Solids 3 (2011) 176–180.
[12] C. Guo, J. Xu, S. Wang, L. Li, Y. Zhang, X. Li, CrystEngComm 14 (2012) 3602–3608.
[13] F.Z. Duan, C. Yan, Q. Ming, Mater. Lett. 65 (2011) 191–193.
[14] L.Q. Mai, F. Yang, Y.L. Zhao, X. Xu, L. Xu, Y.Z. Luo, Nat. Commun. 2 (2011) 1–5.
[15] L. Zhen, W.S. Wang, C.Y. Xu, W.Z. Shao, M.M. Ye, Z.L. Chen, Scr. Mater. 58 (2008) 461–464.
[16] F.B. Cao, L.S. Li, Y.W. Tian, Y.J. Chen, X.R. Wu, Thin Solid Films 22 (2011) 7971–7976.
[17] G. Tian, Y. Chen, J. Zhou, C. Tian, R. Li, C. Wang, H. Fu, CrystEngComm 16 (2014) 842–849.
[18] D. Talla, M. Wildner, A. Beran, R. Škoda, Z. Losos, Phys. Chem. Miner. 40 (2013) 757–769.
[19] F.A. Rabuffetti, S.P. Culver, L. Suescun, R.L. Brutchey, Inorg. Chem. 53 (2014) 1056–1061.
[20] Z.Y. Bao, D.Y. Lei, J. Dai, Y. Wu, Appl. Surf. Sci. 15 (2013) 404–410.
[21] P. Sarker, D. Prasher, N. Gaillard, M.N. Huda, J. Appl. Phys. 114 (2013) 133508.
[22] H. Kato, N. Matsudo, A. Kudo, Chem. Lett. 33 (2004) 1216–1217.
[23] S. Song, Y. Zhang, J. Feng, Y. Xing, Y. Lei, W. Fan, H. Zhang, Cryst. Growth Des. 2 (2009) 848–852.
[24] V.V. Atuchin, O.D. Chimitova, T.A. Gavrilova, M.S. Molokeev, S.J. Kim, N.V. Surovtsev, B.G. Bazarov, J. Cryst. Growth 318 (2011) 683–686.
[25] G. Benoît, J. Véronique, A. Arnaud, G. Alain, Solid State Chem. 13 (2011) 460–476.
[26] Z. Kaminskiene, I. Prosycevas, J. Stonkute, Acta Phys. Pol. A 123 (2013) 111–114.
[27] M. Rycenga, C.M. Cobley, J. Zeng, W. Li, C.H. Moran, Q. Zhang, D. Qin, Y. Xia, Chem. Rev. 111 (2011) 3669–3712.
[28] J. Song, I. Lee, J. Roh, J. Jang, RSC Adv. 4 (2014) 4558–4563.
[29] J. Low, J. Yu, Q. Li, B. Cheng, Phys. Chem. Chem. Phys. 16 (2014) 1111–1120.
[30] C. An, J. Wang, J. Liu, S. Wang, Q.H. Zhang, RSC Adv. 4 (2014) 2409–2413.
[31] L. Ye, J. Liu, C. Gong, L. Tian, T. Peng, L. Zan, ACS Catal. 2 (2012) 1677–1683.
[32] X. Xu, X. Shen, H. Zhou, D. Qiua, G. Zhua, K. Chen, Appl. Catal. A: Gen. 455 (2013) 183–192.
[33] Q. Zhu, W.S. Wang, L. Lin, G.Q. Gao, H.L. Guo, H. Du, A.W. Xu, J. Phys. Chem. C 117 (2013) 5894–5900.
[34] H. Shi, J. Chen, G. Li, X. Nie, H. Zhao, P.K. Wong, T. An, Appl. Mater. Interfaces 5 (2013) 6959–6967.
[35] P. Wang, Y. Tang, Z. Dong, Z. Chen, T.T. Lim, J. Mater. Chem. A 1 (2013) 4718–4727.
[36] W.S. Wang, H. Du, R.X. Wang, T. Wena, A.W. Xu, Nanoscale 5 (2013) 3315–3321.
[37] W.Q. Cui, H. Wang, Y.H. Liang, B.X. Han, L. Liu, J.S. Hu, Chem. Eng. J. 230 (2013) 10–18.
[38] L. Kuai, B. Geng, X. Chen, Y. Zhao, Y. Luo, Langmuir 26 (2010) 18723–18727.
[39] M.A. Butler, J. Appl. Phys. 48 (1977) 1914–1920.
[40] C.H. An, J.Z. Wang, W. Jiang, M.Y. Zhang, X.J. Ming, S.T. Wang, Q.H. Zhang, Nanoscale 4 (2012) 5646–5650.
[41] H. Xu, H.M. Li, J.X. Xia, S. Yin, Z.J. Luo, L. Liu, L. Xu, Appl. Mater. Interfaces 3 (2011) 22–29.
[42] L.S. Zhang, K.H. Wong, Z.G. Chen, J.C. Yu, J.C. Zhao, C. Hu, C.Y. Chan, P.K. Wong, Appl. Catal. A: Gen. 363 (2009) 221–229.
[43] F. Baquero, J.L. Martínez, R. Cantòn, Curr. Opin. Biotechnol. 19 (2008) 260–265.
[44] D.M. Bila, M. Dezotti, Quim. Nova 26 (2003) 523–530.
[45] L.Q. Ye, J.Y. Liu, C.Q. Gong, L.H. Tian, T.Y. Peng, L. Zan, ACS Catal. 2 (2012) 1677–1683.
[46] Y.S. Xu, W.D. Zhang, ChemCatChem 5 (2013) 2343–2351.
[47] C.H. Zhang, L.H. Ai, L.L. Li, J. Jiang, J. Alloys Compd. 582 (2014) 576–582.
[48] C. Chen, W. Ma, J.C. Zhao, Chem. Soc. Rev. 39 (2010) 4206–4219.
[49] Y.X. Tang, Z.L. Jiang, J.Y. Deng, D.G. Gong, Y.K. Lai, H.T. Tay, I.T.K. Joo, T.H. Lau, Z.L. Dong, Z. Chen, Appl. Mater. Interfaces 4 (2012) 438–446.
[50] Y.H. Zhang, Z.R. Tang, X.Z. Fu, Y.J. Xu, J. Appl. Catal. B 106 (2011) 445–452.
[51] R.F. Dong, B.Z. Tian, J.L. Zhang, T.T. Wang, Q.S. Tao, S.Y. Bao, F. Yang, C.Y. Zen, Catal. Commun. 38 (2013) 16–20.